DOI: 10.1002/adma.200601998

Polymer Viscoelasticity and Residual Stress Effects on Nanoimprint Lithography**

By *Yifu Ding*, *Hyun Wook Ro*, *Jack F. Douglas*, *Ronald L. Jones*, *Daniel R. Hine*, *Alamgir Karim*, and *Christopher L. Soles**

Nanoimprint lithography (NIL) is emerging as a patterning technique with enormous potential for nanotechnology. The combination of a resolution of 10 nm or better with the potential to directly pattern functional materials,[1,2] not just sacrificial resist formulations, makes NIL an attractive fabrication process. However, directly patterning such small features raises serious concerns regarding their long-term stability. Factors like surface tension and finite-size effects become significant when the pattern size approaches the nanometer scale. It is well-known that planar polymer films can, under certain circumstances, spontaneously rupture and form droplets when their thickness is reduced to tens of nanometers;[3,4] there are already reports of similar behavior in nanoimprinted patterns.[5,6] Nanostructures fabricated by chemically amplified photoresists display an increased propensity for pattern collapse as their width decreases below 100 nm.[7] Both simulations and experiments seem to indicate that there is a strong reduction in the elastic modulus of a nanostructured material when the feature size decreases below 50 nm.[8,9] Given the potential patterning resolution of NIL, these stability concerns will become increasingly important as even smaller features are realized in a range of different polymers. The direct patterning of functional materials by NIL may necessitate a compromise in resolution to achieve robust and stable nanostructures.

[*] Dr. C. L. Soles, Dr. Y. Ding, Dr. H. W. Ro, Dr. J. F. Douglas, Dr. R. L. Jones, Dr. A. Karim
Polymers Division, National Institute of Standards and Technology
100 Bureau Drive, Gaithersburg, MD 20899-8541 (USA)
E-mail: csoles@nist.gov
D. R. Hine
University of Maryland, Laboratory for Physical Sciences
8050 Greenmead Drive, College Park, MD 20740 (USA)

[**] Official contribution of the National Institute of Standards and Technology (NIST); not subject to copyright in the United States. The error bars presented throughout this manuscript indicate the relative standard uncertainty of the measurement. Certain commercial materials and equipment are identified in order to specify adequately the experimental procedure. In no case does such identification imply recommendation by the National Institute of Standards and Technology nor does it imply that the material or equipment identified is necessarily the best available for this purpose. This work is partially funded by the NIST Office of Microelectronic Programs. Use of the Advanced Photon Source was supported by the U.S. Department of Energy, Office of Science, Office of Basic Energy Sciences, under Contract No. W-31–109-ENG-38. Supporting Information is available online at Wiley InterScience or from the author.

Quantifying the stability of nanoscale structures is, however, a measurement challenge. This requires high-resolution measurements of the 3D pattern shape with nanometer-scale precision, without destroying or cross-sectioning the sample. Most traditional high-resolution shape metrologies fail to simultaneously meet these requirements. To address this challenge we are developing a suite of X-ray-based techniques to quantify pattern shape. These include critical dimension small angle X-ray scattering (CD-SAXS)[10–12] and specular X-ray reflectivity (SXR).[13,14] Here, we utilize the fact that CD-SAXS and SXR can completely characterize the cross section of an imprinted pattern, nondestructively with nanometer-scale resolution, while simultaneously averaging hundreds of nanostructures together for excellent statistics. A description of these shape measurements is provided in the Supporting Information, while more details have been published elsewhere;[10–14] here we focus on the application of these shape measurements for pattern stability. We define the stability of a nanoimprinted structure by measuring its shape change as a function of time in different environments. The real-time shape evolution of nanoimprinted poly(methyl methacrylate) (PMMA) line-and-space patterns has recently been demonstrated with CD-SAXS.[15] A significant decay of the pattern (in terms of a reduction in height and broadening in width) was observed when they were annealed near the glass transition temperature (T_g) of PMMA; however, the decay kinetics were significantly faster than expected and the mechanism for the pattern decay was not entirely clear. Here we show that the pattern decay, especially in high-molecular-mass polymers, is driven primarily by internal stresses that are generated by the nanoimprint process. The origins of these stresses, and methods to control them, are discussed in detail.

Parallel line-and-space patterns are imprinted into PMMA and polystyrene (PS) with varying molecular masses. The characteristics of the polymers, the imprinting conditions, and the shape of the initial patterns are reported in Table 1. All of the lines start with a trapezoidal cross section with a line width of ca. 100 nm and a line height of ca. 165 nm. Table 1 summarizes the exact cross sections, as characterized by CD-SAXS and SXR, in terms of their average line height (H), width (W), sidewall angle (β, $\beta = 0°$ corresponds to a rectangular cross section) and periodicity (Γ) for the as-imprinted patterns. For a given molecular mass polymer, all of the patterns start with nominally identical cross sections.

© 2007 WILEY-VCH Verlag GmbH & Co. KGaA, Weinheim

WILEY InterScience® DISCOVER SOMETHING GREAT

ADVANCED MATERIALS

Table 1. Properties of the polymers used for the nanoimprint and the characterizations of shape of the imprinted line-space grating patterns. The periodicity (Γ), height (H), width (W), and sidewall angle (β) correspond to a trapezoidal cross section used to fit the CD-SAXS data.

Sample (method)	M_n [b] [kg mol^{-1}]	T_g [c] [°C]	T_{imp} [°C]	Γ [nm]	H [nm]	W [nm]	β [d]
PS	24	95.9	146	194.5	168	111	5.7°
(CD-SAXS) [a]	1007	105.3	155	194.5	169	117	5.6°
PS	24	95.9	146	355	165	99	4.5°
(Laser diffraction) [a]	1007	105.3	155	355	165	98	4.4°
	10	119.2	170	355	165	99	4.2°
PMMA	110	126.3	170	355	162	98	4.6°
(CD-SAXS) [a]	518	133.8	184	355	160	99	4.0°

[a] Experiments performed on this type of patterns. [b] All samples are monodisperse. [c] Bulk values determined by differential scanning calorimetry. [d] β is the degree of angular deviation from a perfect rectangular. M_n: number-average molecular weight, T_g: glass transition temperature, T_{imp}: imprint temperature. The standard uncertainties for Γ, H, W, and β are ±0.5 nm, ±5 nm, ±1 nm, and ±0.5°, respectively.

Figure 1 shows CD-SAXS measurements of the real time evolution of the reduced line height ($h = H/H_0$) and width ($w = W/W_0$) for both a series of PS (Fig. 1a) and PMMA (Fig. 1b) patterns of varying molecular mass. The annealing temperature for the PS coincides with the bulk T_g, while the PMMA is approximately 10 °C above its bulk T_g. In agreement with our previous measurements, the patterns decrease in height and broaden in width upon annealing.[15] These rates of change are rapid at first but slow down considerably at longer times. It is noteworthy that both the rate and the extent of the pattern decay are significantly larger in terms of h in comparison with w, consistent with previous observations.[15] Although we do not show the data here, we have confirmed by SXR that the loss in pattern height is accompanied by an increase in the residual layer thickness; volume is nominally conserved.

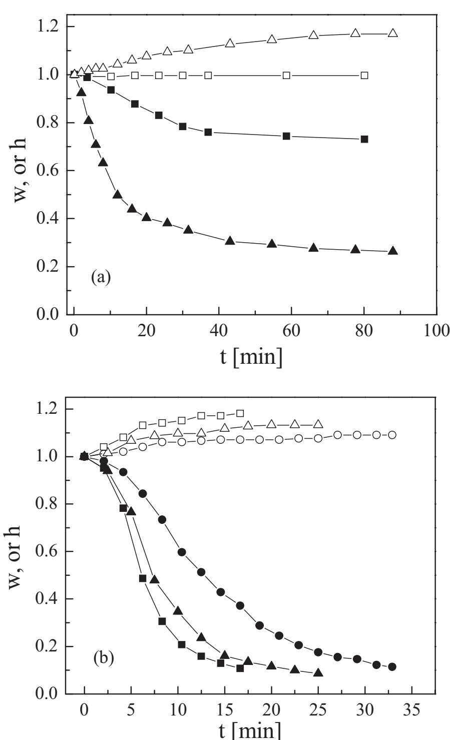

Figure 1. Normalized changes in reduced line height ($h = H/H_o$) and width ($w = W/W_o$) as a function of annealing time for a) PS patterns annealed at T_g and b) PMMA patterns annealed at $T_g + 10$ °C. The open and filled symbols represent the width and height of the pattern lines, respectively. In (a), the squares and triangles correspond to PS24k (where xk refers to the molecular weight of the polymer, see Table 1) and PS1007k patterns, respectively; in (b), the circles, triangles, and squares represent PMMA10k, PMMA110k, and PMMA518k patterns, respectively. The standard uncertainties for H and W are ±5 nm and ±1 nm, respectively.

The most striking observation, however, is that the initial rate of pattern change is much faster in the high-molecular-mass (entangled) samples for both PS and PMMA (Fig. 1). When the PS patterns are annealed at their bulk T_g, the line height of the PS1007k (where xk denotes the molecular mass of the polymer, see Table 1) sample decays to more than 70 % of its original value within an hour, compared to a less than 30 % reduction in height for the PS24k pattern (Fig. 1a). For patterned PMMA films annealed at $T_g + 10$ °C, the differences between the three molecular mass samples are less pronounced, but the same trend is observed: higher molecular masses decay faster (Fig. 1b). It is also apparent that the discrepancy between the height and width decay is greater in the PMMA samples. After 30 min, the lines have decayed by 90 % in terms of their initial height, with almost no change in the pattern width. The pattern decay is highly anisotropic, especially for the high-molecular-mass polymers.

For a pattern heated above the T_g of the polymer, surface tension (γ) will tend to smooth out the features of the pattern; a flat surface is thermodynamically stable.[16,17] The γs for the different PS (and PMMA) samples in Table 1 show negligible differences with molecular mass.[18] Because all of the imprinted patterns within each PS or PMMA series start with an identical cross section, the surface-tension component of the driving force for pattern decay should not change with molecular mass. By contrast, the kinetics of the pattern decay in response to the thermodynamic driving force are determined by the shear viscosity (η_0, see Eq. 2), which strongly depends on the molecular mass. For polymeric melts there is a transition from $\eta_0 \propto M^1$ to $\eta_0 \propto M^{3.4}$ at a critical entanglement molecular mass, M_c ($M_c \approx 30$ kg mol^{-1} for bulk PS).[19] From γ and η_0 alone, one would expect the decay rate of PS1007k to be several orders of magnitude slower than that of the PS24k imprinted film; however, exactly the opposite trend is observed: the higher-molecular-mass patterns decay faster (Fig. 1). This is inconsistent with a simple surface-tension-driven viscous

 © 2007 WILEY-VCH Verlag GmbH & Co. KGaA, Weinheim

flow mechanism governing the pattern decay near the T_g. Rather, the viscoelastic properties of the polymer during the mold-filling processes are implicated to explain this interesting pattern decay behavior.

The substantially greater viscosities of the high-molecular-mass PMMA and PS also make it more difficult to fill the mold with the molten polymer during the imprint process at $T_g + 50\,°C$ (see Experimental). The nanoimprint mold-filling process is undoubtedly a complicated rheological process. In general, we can expect the polymer deformation to be inhomogeneous because of the pattern geometry. Both the strain magnitudes and rates may vary from point to point in the different regions of the mold during the imprint.[19] For a highly entangled polymer, it is reasonable to anticipate both elastic and plastic deformation of the material during this process. The plastic deformation can also vary from point to point, ranging from shear in some regions to extensional flow in others.[20] Simulations suggest that when the residual layer of resist between the pattern and the supporting substrate is thicker than the width of penetrating protrusions in the mold, shear flow will dominate the mold filling.[21] The molds and thicknesses of the films imprinted here are consistent with this shear-flow-dominated regime. It has been suggested that the shear rates during the imprinting process approach the shear-thinning regime, especially for higher-molecular-mass polymers.[20,22] Therefore, comparing the time scale for structural relaxations in the bulk polymer to the duration of the imprint process provides some insight into the mold-filling physics.[23] This is done below just for the PS patterns, given the abundant literature on the rheological properties of PS for a range of molecular masses.

For an approximate characterization of the shear flow of PS during the imprint process, we use the bulk terminal relaxation time $\tau_t = J_e^0 \eta_0$, where J_e^0 is the steady-state compliance and η_0 is the zero-shear viscosity. Physically, τ_t reflects the longest time required for the polymer to relax entanglement constraints and enable flow.[19] Typically, J_e^0 is temperature independent near the imprint temperatures reported in Table 1; we use J_e^0 values of 2.51×10^{-6} Pa^{-1} and 1.38×10^{-5} Pa^{-1} reported at 160 °C for PS24k and PS1007k, respectively.[24] The classic Vogel–Fulcher–Tammann (VFT) equation is then used to estimate η_0 as

$$\eta_0 = A \exp\left(\frac{B}{a_f (T - T_\infty)}\right) \tag{1}$$

where A, B, and a_f represent empirical fitting constants and T_∞ is the Vogel temperature, at which the viscosity diverges to infinity. The estimate is made by selecting values of A, B, a_f, and T_∞ from the literature that are appropriate for the molecular masses of the PS used here.[24] The resulting estimates of η_0 are 5.4×10^3 Pa s and 2.4×10^8 Pa s for PS24k and PS1007k, respectively, at their imprinting temperatures of $T_g + 50\,°C$. The corresponding τ_t values were estimated to be on the order of 10^{-2} s and 3000 s, respectively. By comparing τ_t with the imprint time $\tau_{imp} \approx 5$ min $= 300$ s (see Experimental), we see that $\tau_t \ll \tau_{imp}$ for PS24k at $T_g + 50\,°C$. Consequently, PS24k should have ample time to relax internal stresses related to the deformation and/or flow of the material into the mold. This is not surprising given our η_0 estimate; 5.4×10^3 Pa s is on the same order of magnitude as the viscosity of glycerol at room temperature. However, the η_0 estimate of 2.4×10^8 Pa s for the PS1007k sample is eight orders of magnitude more viscous than water, similar to the viscosity of tar or pitch at room temperature. Filling the mold with PS1007k at $T_g + 50\,°C$ would therefore require considerable elastic/plastic deformation and/or a significant reduction in the effective viscosity by shear thinning. Because the stress relaxation time is much longer than the imprinting time, i.e., $\tau_t \approx 3000\ s \gg \tau_{imp} = 300$ s for PS1007k at this temperature, any internal stress or molecular bias associated with the deformation would not be able to relax within the duration of the imprinting. With fast cooling under a relatively large imprint pressure (3.4 MPa), these stresses are frozen into the resulting glassy structures. These internal stresses are expected to influence the pattern shape evolution when the pattern is then separated from the mold.[25]

From the above discussion, it is clear that the stresses acting on PS1007k patterns include both the nonequilibrium internal stresses induced by the imprinting process and the surface tension, so that the driving force for the pattern decay is more complicated for temperatures near T_g. This complexity is revealed in laser diffraction experiments. The PS patterns in Figure 1a, with a periodicity of (194.5 ± 0.5) nm are below the diffraction limit for a typical visible laser, but the mold with a pitch of (355.0 ± 0.5) nm (Table 1) will produce a first-order diffraction peak from a violet laser ($\lambda = 405$ nm) at a diffraction angle 2θ of approximately 70°. The lines have nearly the same cross section as the patterns in Figure 1a, with the exception of the approximately 1:3 versus 1:1 line-to-space ratio (see Table 1). Patterns of both the PS24k and PS1007k were imprinted with this mold under identical conditions as the PS sample in Figure 1a. The intensity of the first-order diffraction spot is monitored in situ while annealing the patterns at $T_g + 8\,°C$. There are advantages and disadvantages to employing visible versus X-ray radiation to characterize the imprinted patterns. The measurements are easily performed over long periods of time (days) in the laboratory, which is generally not feasible at a synchrotron. Although the intensity of the scattered radiation is directly related to the amount of material in the pattern, it is nearly impossible to quantitatively extract the pattern shape when the features are small compared with the wavelength of the light. Here we use the convenience of the laser diffraction method to characterize the general timescales of the decay, without worrying about the precise pattern shape.

Figure 2 shows the first-order diffraction intensity I as a function of annealing time at $T_g + 8\,°C$ for both PS patterns on a log–log plot. For comparison, the normalized height change of the PS1007k sample from Figure 1a is included (solid line). Both samples display a strong decay of I upon annealing. Consistent with Figure 1, the initial decay of PS1007k is

 © 2007 WILEY-VCH Verlag GmbH & Co. KGaA, Weinheim

ADVANCED MATERIALS

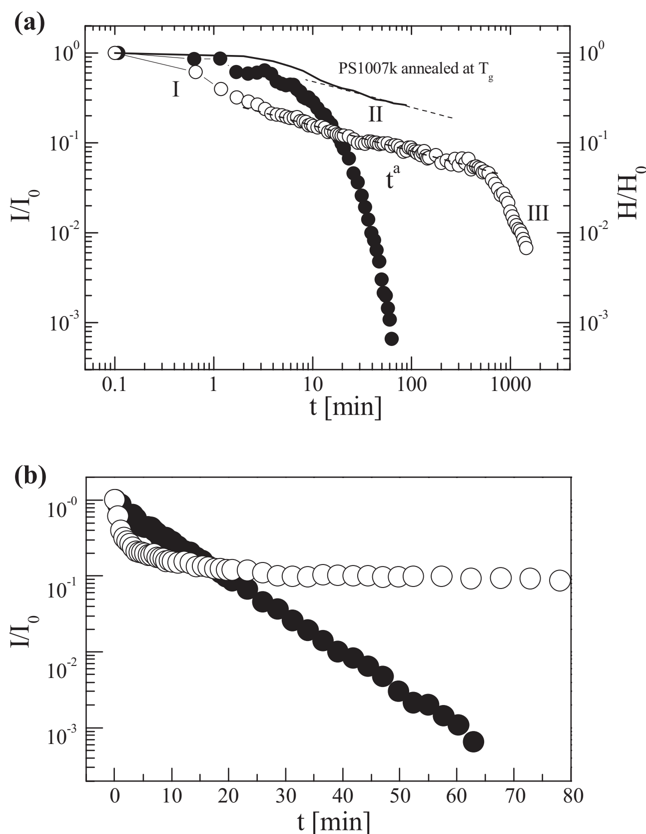

Figure 2. Intensity variations (normalized by the initial intensity before annealing, I_0) of the first-order laser diffraction peak shown as a function of annealing time for the PS24k (●) and PS1007k (○) patterns at $T_g + 8\,°C$. Part (a) shows these variations in a log–log representation, while (b) presents the data in a semi-log format. The dashed line in the log–log portion of the graph (a) is a linear fit defining the power law decay of regime II, with a slope of approximately –0.3. The solid line corresponds to the height changes for the PS1007k sample annealed at T_g for PS1007k measured by CD-SAXS (same data as in Fig. 1a). The standard uncertainty in the intensity measurements is negligible compared with the size of the data symbols.

still faster than PS24k, but shifted to shorter time scales with the increase of annealing temperature (T_g for Fig. 1 versus $T_g + 8\,°C$ for Fig. 2). The most interesting observation, however, is the difference between the intensity variations at longer times; obtaining this data by CD-SAXS was not practical because of the relatively long measurement time that would be required. The PS24k pattern shows a single exponential decay over the entire time range (linear slope on the semi-log representation in part b of Fig. 2), while the PS1007k pattern shows three distinct decay regimes: a short initial period of fast decay (regime I), an extended intermediate region characterized by a slower power-law decay (regime II), finally giving way to what appears to be an exponential decay at long times (regime III).

Hamdorf and Johannsmann studied the role of surface-tension-driven decay of patterned surfaces in PS and PMMA above the T_g.[16] In their case, sinusoidal gratings with a periodicity of 600 nm and a very shallow amplitude (ca. 5 nm) were thermally embossed into the surface of bulk polymers. With the assumption that surface tension is the only driving force, they predict that the amplitude of the gratings will decay exponentially with time. The relaxation time of this exponential decay is determined by γ, the periodicity of the pattern (Γ), and the shear viscosity of the material (η) as[16]

$$\tau_d = \eta\Gamma/\pi\gamma \tag{2}$$

We can apply this model to the decay of our high-aspect-ratio features as a crude approximation. Exponential fits to the data in Figure 2 yield decay time constants of $\tau_d = 8.3$ min for the PS24k (entire time range) and $\tau_d = 664$ min for PS1007k in regime III. To estimate the viscosity, we utilize a value of $\gamma \approx 33$ mN m^{-1} for both patterns at their annealing temperature.[18] With these parameters and Equation 2, we estimate the viscosities of the PS24k and PS1007k at $T_g + 8\,°C$ to be 1.5×10^8 Pa s and 2×10^{10} Pa s, respectively. These η values can be compared to the VFT predictions for the bulk viscosities at the same temperatures (again by using Eq. 1 and literature parameters[24]), which are 2.7×10^8 Pa s and 1.1×10^{12} Pa s for PS24k and PS1007k, respectively. The viscosity for PS24k predicted by VFT is of the same order of magnitude as the effective viscosity measured by τ_d, indicating that the pattern decay mechanism is primarily surface-tension-induced viscous flow. This is consistent with the previous estimate that $\tau_t \ll \tau_{imp}$ for PS24k. Stresses that may have been induced as the mold pressed into the film have sufficient time to relax over the duration of the imprint process. However, the VFT model predicts a viscosity for the PS1007k patterns that is about two orders of magnitude greater than what would be experimentally estimated from τ_d; at long times the high-molecular-mass pattern decays much faster than what would be predicted on the basis of surface tension and viscosity. This is consistent with $\tau_t \gg \tau_{imp}$ for the PS1007k and a slow recovery of the sheared glassy melt viscosity after shear thinning.[26]

We interpret the fast changes of the normalized intensity (or H) at short times (regime I of Fig. 2) of the PS1007k pattern as an elasticlike response of the polymer deformed by the imprint process in response to a combination of the residual stress and surface tension. Because response occurs on a timescale significantly longer than the segmental relaxation time ($\tau_a \approx 0.01$ s),[27] this recovery must be associated with the entropic elasticity of a highly deformed and highly entangled polymer in the rubbery state. The deformation will distort the chain conformations away from their equilibrium conformations, leading to the entropic elasticity as in the familiar case of stretching a rubber band. This analogy with a stretched rubber band should not be surprising given the relatively large viscosity (tar- or pitchlike) of PS1007k at the imprint temperature and the long stress relaxation time (τ_t) of the polymer melt compared with the duration of the imprint; chain distortions simply do not have time to relax. Deep in the glassy state, the material is too stiff to relax or dissipate this driving

© 2007 WILEY-VCH Verlag GmbH & Co. KGaA, Weinheim

force.[28] However, when the sample is heated near T_g the modulus that resists this entropic force dramatically decreases and the rubberlike elastic recovery is observed.

The large strains created by the short-time elastic deformation can be expected to build up until yield occurs, followed by a regime of plastic flow. In the post-elastic deformation regime (regime II), the intensity decay of PS1007k exhibits a power-law decay with annealing time with an average exponent of approximately –0.3, consistent with some type of post-yield flow process. (For comparison, the normalized height change of the PS1007k from Fig. 1a is also plotted in Fig. 2.) Although the annealing times for the decay data from the CD-SAXS measurements are not as extensive, a similar power law tail with a slope of –0.3 seems reasonable at the long times. This power-law decay is characteristic of the Andrade creep phenomenon, where the shear compliance ($J(t)$) scales as $J(t) \propto t^{1/3}$. The term "creep" refers to the long-term flow of a viscoelastic material under a constant stress or load. While Andrade creep was originally observed in metallic materials,[29] this phenomenon is also prevalent in polymer materials, where two different types of Andrade creep behavior have been identified. The first type of creep deformation is found in glassy polymers, regardless of whether they are entangled or not,[30] and not of interest here. The second type of Andrade creep behavior is unique to highly entangled (molecular masses above M_c) polymers fluids at timescales longer than their glassy or elastic response time, but shorter than the timescale associated with the viscous flow of the terminal regime (characterized by τ_t);[19,31] this is characteristic of creep in the rubbery plateau regions. Because the $t^{-1/3}$ decay is only found in PS1007k (PS24k is just below the bulk critical entanglement molecular mass) above the T_g, it is reasonable to identify this process as the creep recovery in Figure 2.

Finally, at longer times we observe an exponential-like decay of the scattering intensity in regime III that is consistent with the viscous flow of the terminal regime. As mentioned previously this behavior is consistent with a simple Newtonian liquid, and Equation 2 can be used to estimate the apparent shear viscosity η from the exponential decay constant. However, in regime III the resulting viscosity from the PS1007k pattern decay kinetics is significantly lower (by about two orders of magnitude) than would be predicted from the bulk viscosity of the unsheared fluid. A significantly reduced viscosity compared to the quiescent values, η_0, is expected to arise from the stress shear thinning during the imprinting process. The apparent two orders of magnitude lower viscosity estimated from regime III would be consistent with extremely slow recovery of the melt to the properties of the quiescent fluid.[19,26]

The important implication of these findings for practitioners of the thermal embossing form of NIL is to consider these internal stresses and their potential impact on the intended function of the imprinted pattern. Here we "accelerated" the pattern decay to timescales that were suitable for characterization by heating the samples to near T_g values. However, creep or stress relaxation behaviors are common in polymers even well below the T_g, potentially raising stability concerns at room temperature. These concerns will become increasingly important as the feature sizes continue to shrink and the materials that are imprinted move away from resist formulations that are sacrificial, i.e., do not have to remain stable for very long periods of time. There is also a general notion within the NIL community to reduce the imprint temperature to a value as close to room temperature as possible. Low-temperature imprints minimize thermal distortions of the substrates, coefficient of thermal expansion mismatch issues, and shrinkage effects upon cooling. This generally means tuning the T_g value of the resist formulation to be close to room temperature. However, the proximity of the T_g value to room temperature also increases the propensity for the structures to relax their process-induced stresses, possibly leading to long-term stability issues. Finally, there are reports showing that when imprinting very small features with a high aspect ratio, high-molecular-mass polymers are superior in terms of their cohesive strength; the low-molecular-mass analogs have a greater propensity to shear off or show cohesive failure during mold separation.[6] The knowledge developed here illustrates that the increased cohesive strength must also be balanced against increased levels of residual stress in the patterns.

Experimental

Nanoimprint Pattern Fabrication: PS and PMMA with a range of different molecular masses, as indicated in Table 1, were purchased from Polymer Laboratories. Solutions of PS and PMMA were prepared in toluene and anisole, respectively. Films were first spun-cast at 209 rad s^{-1} (2000 rpm) onto clean Si wafers with a native oxide surface and then annealed at 170 °C for 30 min to remove the residual solvent. The imprint masters with parallel line-and-space gratings were fabricated by interference lithography and etched into silicon oxide. To facilitate the mold release, a low-energy fluorinated self-assembled monolayer was applied to the mold. All imprints were made on a Nanonex NX-2000 tool. To create the pattern, the tool was heated to the imprint temperature of $T_{imp} = T_g + 50$ °C while applying a pressure of 3.4 MPa for 5 min. The tool was cooled to 55 °C before releasing the pressure and separating the mold from the imprinted pattern. For all of the samples the polymer completely filled the mold, leaving a residual layer of approximately 200 nm beneath the film.

Pattern Shape Characterization: Principles and applications of CD-SAXS and SXR to precisely determine the imprinted pattern shape and evolution are described in the Supporting Information. Additional details have been previously described elsewhere [10–14].

Laser Diffraction Experiments: Laser diffraction experiments were set up in reflection geometry. The sample was mounted horizontally on a hot stage (Linkam THMS600) with precise temperature control (Linkam TMS94). The wavelength of the laser was 405 nm, and the polarization of incident radiation was parallel to the grating lines. The scattering intensity of the first-order diffraction peak at a scattering angle 2θ of approximately 70° was recorded with a charge coupled device (CCD) camera as a function of the annealing time and normalized against fluctuations in beam intensity.

Received: September 1, 2006
Revised: December 22, 2006
Published online: April 20, 2007

© 2007 WILEY-VCH Verlag GmbH & Co. KGaA, Weinheim

[1] M. D. Austin, H. X. Ge, W. Wu, M. T. Li, Z. N. Yu, D. Wasserman, S. A. Lyon, S. Y. Chou, *Appl. Phys. Lett.* **2004**, *84*, 5299.
[2] F. Hua, Y. G. Sun, A. Gaur, M. A. Meitl, L. Bilhaut, L. Rotkina, J. F. Wang, P. Geil, M. Shim, J. A. Rogers, A. Shim, *Nano Lett.* **2004**, *4*, 2467.
[3] G. Reiter, *Phys. Rev. Lett.* **1992**, *68*, 75.
[4] J. Bischoff, D. Scherer, S. Herminghaus, P. Leiderer, *Phys. Rev. Lett.* **1996**, *77*, 1536.
[5] Y. Hirai, S. Yoshida, N. Takagi, *J. Vac. Sci. Technol. B* **2003**, *21*, 2765.
[6] Y. Hirai, S. Yoshida, N. Takagi, Y. Tanaka, H. Yabe, K. Sasaki, H. Sumitani, K. Yamamoto, *J. Appl. Phys.* **2003**, *42*, 3863.
[7] H. B. Cao, P. F. Nealey, W. D. Domke, *J. Vac. Sci. Technol. B* **2000**, *18*, 3303.
[8] K. Van Workum, J. J. de Pablo, *Nano Lett.* **2003**, *3*, 1405.
[9] C. M. Stafford, B. D. Vogt, C. Harrison, D. Julthongpiput, R. Huang, *Macromolecules* **2006**, *39*, 5095.
[10] R. L. Jones, T. Hu, E. K. Lin, W. L. Wu, R. Kolb, D. M. Casa, P. J. Bolton, G. G. Barclay, *Appl. Phys. Lett.* **2003**, *83*, 4059.
[11] T. J. Hu, R. L. Jones, W. L. Wu, E. K. Lin, Q. H. Lin, D. Keane, S. Weigand, J. Quintana, *J. Appl. Phys.* **2004**, *96*, 1983.
[12] R. L. Jones, T. J. Hu, C. L. Soles, E. K. Lin, W. Hu, R. M. Reano, S. W. Pang, D. M. Casa, *J. Microlithogr. Microfabr. Microsyst.* **2005**, *5*, 013 001.
[13] H. J. Lee, C. L. Soles, H. W. Ro, R. L. Jones, E. K. Lin, W. L. Wu, D. R. Hines, *Appl. Phys. Lett.* **2005**, *87*, 263 111.
[14] H. J. Lee, H. W. Ro, C. L. Soles, R. L. Jones, E. K. Lin, W. L. Wu, D. R. Hines, *J. Vac. Sci. Technol.* **2005**, *23*, 3023.
[15] R. L. Jones, T. J. Hu, C. L. Soles, E. K. Lin, R. M. Reano, S. M. Casa, *Nano Lett.* **2006**, *6*, 1723.
[16] M. Hamdorf, D. Johannsmann, *J. Chem. Phys.* **2000**, *112*, 4262.
[17] E. Buck, K. Petersen, M. Hund, G. Krausch, D. Johannsmann, *Macromolecules* **2004**, *37*, 8647.
[18] G. T. Dee, B. B. Sauer, *Adv. Phys.* **1998**, *47*, 161.
[19] J. D. Ferry, *Viscoelastic Properties of Polymers*, 3rd ed., John Wiley & Sons, New York, **1980**.
[20] H. Schulz, M. Wissen, N. Bogdanski, H. C. Scheer, K. Mattes, C. Friedrich, *Microelectron. Eng.* **2006**, *83*, 259.
[21] H. D. Rowland, A. C. Sun, P. R. Schunk, W. P. King, *J. Micromech. Microeng.* **2005**, *15*, 2414.
[22] Z. N. Yu, H. Gao, S. Y. Chou, *Appl. Phys. Lett.* **2004**, *85*, 4166.
[23] H. C. Scheer, N. Bogdanski, M. Wissen, T. Konishi, Y. Hirai, *J. Vac. Sci. Technol. B* **2005**, *23*, 2963.
[24] J. C. Majeste, J. P. Montfort, A. Allal, G. Marin, *Rheol. Acta* **1998**, *37*, 486.
[25] O. Takeshi, K. Sekimoto, *Phys. Rev. Lett.* **2005**, *95*, 108301.
[26] R. A. Stratton, A. F. Butcher, *J. Polym. Sci. Polym. Phys. Ed.* **1973**, *11*, 1747.
[27] P. G. Santangelo, C. M. Roland, *Macromolecules* **1998**, *31*, 4581.
[28] C. M. Stafford, C. Harrison, K. L. Beers, A. Karim, E. J. Amis, M. R. Vanlandingham, H. C. Kim, W. Volksen, R. D. Miller, E. E. Simonyi, *Nat. Mater.* **2004**, *3*, 545.
[29] E. N. Da C. Andrade, *Proc. R. Soc. Ser. A* **1910**, *84*, 1.
[30] L. C. E. Struik, *Physical Ageing in Amorphous Polymers and Other Materials*, Elsevier, Amsterdam, **1978**.
[32] D. J. Plazek, N. Raghupathi, V. N. O'Rourke, *J. Polym. Sci. Polym. Phys. Ed.* **1980**, *18*, 1837.
[33] L. G. Parratt, *Phys. Rev.* **1954**, *95*, 359.

© 2007 WILEY-VCH Verlag GmbH & Co. KGaA, Weinheim